Robust Design of a 3D- and Inkjet-Printed Capacitive Force/Pressure Sensor

Lisa-Marie Faller and Hubert Zangl
Sensors and Actuators Department
Alpen Adria University Klagenfurt
Klagenfurt, Austria
Email: lisa-marie.faller@aau.at

Abstract

We present a method to robust design of a capacitive force/pressure sensor, manufactured in rapid prototyping manner, by adaptation of the electrode structure. Rapid prototyping technologies, such as the considered 3D- and inkjet-printing processes, suffer from major uncertainties in geometry and material properties. The presented methodology consequently aims at minimizing the influence of topology and geometry variations as well as measurement noise on the sensor read-out. It is outlined as a consequence of the beneficial combination of a Latin Hypercube design of experiments and the subsequent Linear Bayesian Minimum Mean Square Error (BMSE) estimator. Even though the additional effort in hardware and signal processing is low, we demonstrate a significant improvement of the measurement uncertainty when we move from a single capacitor to an optimized capacitor array.

1. Introduction

Sensing of pressure and/or force is a relevant topic with versatile application areas ranging from wearable electronics [1] and robotics [2] to medical [3], [4]. Capacitive sensing enables high resolution sensing in combination with high bandwidth and excellent linearity [5], [6]. Furthermore the capacitive technology offers production-related advantages such as low-cost designs with basic structures being readily manufactured with, e.g. printing processes.

3D printing technology nowadays offers comparatively good accuracy at moderate costs and has thus become attractive for realization of functional components in particular for prototypes and low volume products [7]. As an attractive feature, sensing elements can be part of the packaging of the devices and withstand harsh environmental conditions. Inkjet-printing provides, in general, great potential for electronics manufacturing and sensors in particular [8].

Despite the advantages for rapid prototyping, both printing processes suffer from tolerances in excess of those from standard processes such as deposition or Printed Circuit Board (PCB) fabrication. To us it is thus mandatory to evaluate design criteria with respect to variations in topology (size, accurate positioning) as well as boundary conditions (uniform pressure vs. force on differing areas and locations) and material properties (conductivity, linearity, deformation hysteresis). Essentially aiming at an improvement of the sensor system as a whole to compensate for the inferior quality of the sensing facility itself (compare [9]). For this work, Finite Element Model (FEM) simulations of the capacitive device are structured following a Design Of Computer Experiments (DOCE) targeted at determining an optimal calibration process for the considered sensor structure. The novelty lies in the suggestion to employ DOCEs and statistical signal processing in a dedicated way, combining beneficial properties of both, leading to an overall robust sensor design.

A 3D-printed steel diaphragm for force/pressure sensing [10] was realized applicable as, e.g. part of a 3D-printed housing for an entire device, allowing for use in harsh environments. Capacitive sensing electrodes in different configurations are available in an inkjet-printed topology on PET-foil and as rigid-support PCB-design. In the experiments, force is applied in direction of the normal vector to diaphragm-plane, using a specifically designed setup. Results are gathered for a single-ended PCB structure as well as a printed device.

2. System Description and Simulation Setup

The whole system is comprised of a circular 3D-printed steel diaphragm superposed to an inkjet-printed electrode structure. The axially symmetric design is supposed to be advantageous with respect to geometrical variations such as rotation. The steel diaphragm is depicted in Figure 1 and an illustration of how the measurand (here: force) should ideally act on the topology is given in Figure 2. While the schematic illustration treats the system's usage as force sensing device, an adaptation to pressure sensing is possible by applying a uniform force to the entire diaphragm surface and norming it to the surface area.

A. Sensing Principle

Capacitive sensors can be designed to work in either single-ended or differential mode. In both modes, the change in capacitance between conductive surfaces, i.e. electrodes, at different electric potentials, is measured. Applying a voltage to one electrode, consequently called transmitter, and measuring the resulting displacement current in a second electrode, i.e. the receiver, is termed differential mode. In a single-ended design, the displacement current at the transmitter is determined. Measurements in

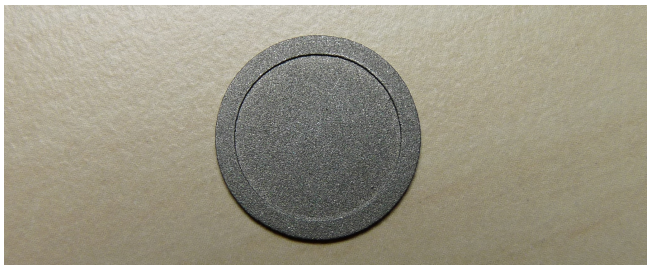

Figure 1. 3D-printed steel diaphragm incorporating the sensing element as well as the sensor housing making the device robust against environmental influences.

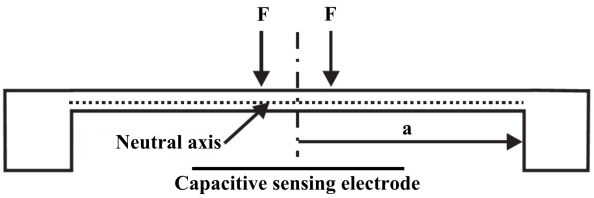

Figure 2. Schematic of the idealized pressure sensing system. The nominal action of the force is at the center of the diaphragm, in normal direction of the diaphragm plane, with a the radius of the diaphragm.

single-ended mode are possible to the open environment or distant ground.

In the target design, the bottom electrode is used as transmitter while the steel housing incorporates the receiver and are assumed to form a structure resembling a parallel plate capacitor describable by the following simplified model

$$\Delta C = \frac{\varepsilon_0 \varepsilon_r A_r}{\Delta d} \tag{1}$$

where ΔC is the change in capacitance in farads, A_r the active plate area in square meters, ε_0 the dielectric constant of vacuum, ε_r the relative dielectric constant of the material between the plates and d the plate spacing in meters. We consider an inkjet-printed sensor front-end employing single-ended, or self-capacitance measurement mode [6] which offers better SNR than a differential system. Justified by the system settings which allow for a hermetically sealed sensor package, we leave disadvantageous environmental influences such as dew or moisture and electromagnetic compatibility issues [11] disregarded. The use of diaphragms is common practice in pressure sensing and is therefore well-studied [12], [13] and [14].

B. FEM Simulation

A commercial multiphysics-capable software tool is used to draw the topology, assign materials and assemble and solve for the relevant physics and couplings. In the first step, the system geometry is realized in a parametrized design providing for the flexibility necessary in the optimization procedure.

As shown in Figure 3, the electrode is realized as conductive surface on which an array of symmetrically

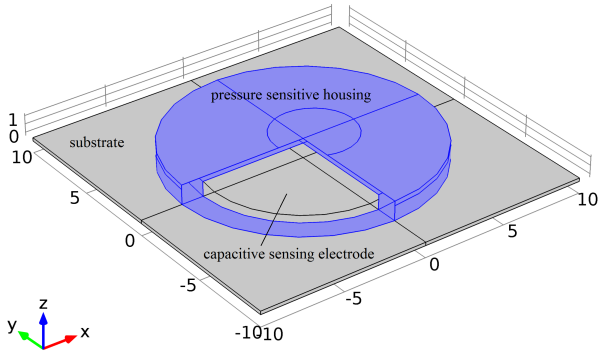

Figure 3. System topology where one quarter of the design is hidden to illustrate the electrode structure below the force sensitive circular diaphragm (blue domain).

(with respect to radius) distributed points is defined. The electrode surface is designed to cover the entire space below the diaphragm, respecting tolerances at the rim in order not to contact the diaphragm. The point-wise evaluation allows to assemble electrode structures off-line, i.e. after simulating once, it will thus be needless to rerun simulations to cover various topologies. The conductivity s_{var} of the conductor material is considered as variable.

The diaphragm itself is designed as closed circular plane on a radial support made of cast iron. Variable geometry parameters of the housing are the support thickness (, i.e. its height) $t_{support}$, the plane thickness t_{dia}, its (outer) radius r_{dia}, the inner radius r_{in}. Material parameters considered subject to uncertainties are the modulus of elasticity E_{var}, the Poisson ratio ν_{var} and the material density ρ_{var}.

To guarantee for flexibility in boundary conditions, a parametrized surface at the top of the diaphragm is realized as shown in Figure 4. Design variables with regard to this surface are the surface diameter (active diameter) f_{dia}, its distance from the center on the x-axis f_{xoffs}, the distance from the diaphragm center on the y-axis f_{yoffs} and the applied normal force F. This simulation setup is adequate to also cover forces non-normal to the diaphragm plane since these can always be transformed to equivalent normal forces in a suitably changed coordinate system, i.e. simulated by movement of the active diameter.

The equations solved for the FEM simulations are on the one hand Cauchy's momentum equation which gives the deformation of elastic material under external loads assuming no electric field

$$\rho \frac{d^2 p}{dt^2} = \nabla T_M + F_{ext} \tag{2}$$

with density ρ, p defining the location of a point fixed in the material at time instance $t = 0\,\mathrm{s}$, T_M the stress

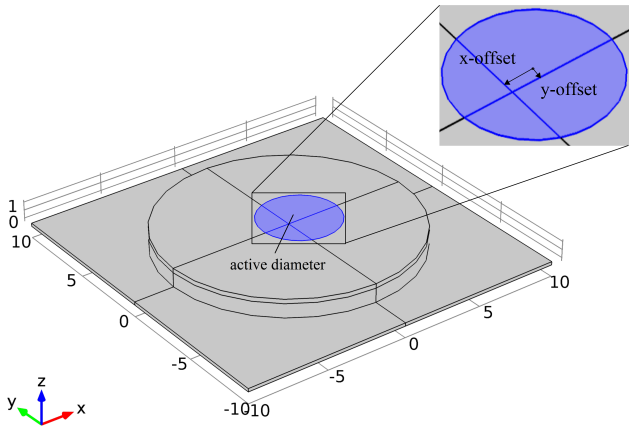

Figure 4. Entire system geometry, illustrating the parametrized surface to which the force is applied (blue surface).

tensor and F_{ext} is an external volume force. The stress due to an electrostatic field can be computed employing the Maxwell stress tensor T_{EM} given by

$$T_{EM} = \left(\frac{1}{2}\varepsilon_0 EE\right) I_T + \varepsilon_0 EE^T \tag{3}$$

with I_T the identity tensor, E the electric field and ε_0 the permittivity of vacuum, where a coupling of both is reached through a continuity equation

$$n_{EM}(T_M - T_{EM}) = 0 \tag{4}$$

which, using n_{EM} the outside normal vector to the domain where the electrostatics are valid, essentially constrains stress to be continuous across stationary boundaries of adjacent materials. Finally, in the region of the model, where an electric field is assumed, Gauss law is solved

$$\nabla D = \rho_V \tag{5}$$

with $D = \varepsilon_0 E$ the electric displacement field and ρ_V the space charge density [15].
First the deformation of the diaphragm is computed and then propagated to the electrostatics equations which is then solved based on the new geometric configuration.

3. Optimization Approach

It is generally true for capacitive sensors that they are capable of detecting any parameter variation which produces a change in capacitance. In order to avoid indicating a change in capacitance due to a parameter which is not the measurand, several ways of system optimization can be employed. The usage of all-printed devices, facilitating rapid prototyping, as we do here, excludes optimization methods which aim at designing the optimal geometry already beforehand. The uncertainties originating from production can neither be predicted nor prevented. To still guarantee for a system, fulfilling robust design optimality criteria, although suffering from major tolerances concerning geometry and material, we base our optimization procedure on a tight coupling of the previously documented field numerical and following statistical methods.
We expect variations to be not only in the sensor design, but also in the way the measurand acts on the system. The sensor is designed to accept force or pressure applied at its center in a direction normal to the diaphragm plane. In real world applications this might not be achieved due to inaccuracies (physical constraints) in the sensor mounting. Furthermore, material properties may vary, e.g. due to environmental conditions such as weather, temperature or human influences. In a robust sensor design, the indicated value shall still reflect the true value as accurate as possible. To provide for such a behaviour, we start with the definition of the measurement vector as a function of the measurand θ, design parameters ξ and nuisance variables τ. Our aim is to optimize the design for the complete set of producible devices, we thus consider the measurand and nuisance parameters as Random Variables (RVs), then the measurement y can be given as realization of the random vector

$$Y = g(\theta, \xi, \tau) + N \tag{6}$$

where g reflects a deterministic part and random influences are gathered in N. A certain distribution F is assumed for the nuisance parameters τ. For the target system, variables related to the electrode topology are considered as design parameters, uncertainties in geometry, material and action of force are of the category of nuisance parameters.
In the next step, the measurand or state vector θ is to be reconstructed based on the formulation of the measurement vector y. The result is an estimate of the state vector as a function of the measurement $\hat{\theta} = h(y)$, which essentially defines the calibration curve of the sensor. We further refer to this as an estimator for the true value of the measurand.
Although it is, in certain cases, possible to analytically determine the functional dependency, this is seldom done in applications. A reason for this is complexity and uncertainty in parameters. Often, we do not know beforehand about geometrical and topological uncertainties, but we know properties of their distributions such as the mean and variance, i.e. tolerances as given by the manufacturer. Having such information at hand, together with the knowledge of the distribution of the parameter to be estimated, this allows to construct a Bayesian mean square error estimator. Estimators based on the Bayesian approach are beneficial since they firstly allow for consideration of prior knowledge. Secondly, they yield the best estimator when the Minmum Variance Unbiased Estimator (MVUE) cannot be determined uniquely and thirdly, they facilitate estimation of only one parameter of interest while several are considered unknown, i.e. random. For the target setup, many estimators may exist, which are optimal with respect to a certain point (geometrically or with respect

to the application of the measurand) of the design, but the Bayesian methodology will yield an estimator which results in the best 'on average' for the entire domain [16]. Such an estimator, i.e. the Minimum Mean Square Error (MMSE) estimator, is found by minimizing the Bayesian mean square error (Bmse)

$$Bmse([\hat{\theta}]_i) = E\{\theta_i - \hat{\theta}_i^2\} \tag{7}$$

$$= \int\int (\theta_i - \hat{\theta}_i)^2 p(y,\theta_i) d\theta_i dy \tag{8}$$

with $p(y,\theta_i)$ the formerly joint probability density function (pdf) marginalised over all $\theta_j \neq \theta_i$ and E denotes the expectation operator, then explicitly,

$$\hat{\theta} = \int \theta p(\theta|y) d\theta = E\{\theta|y\} \tag{9}$$

where $p(\theta|y)$ denotes the conditional pdf of θ conditioned on y and can be determined using Bayes's theorem

$$p(\theta|y) = \frac{p(y|\theta)p(\theta)}{\int p(y|\theta)p(\theta)d\theta} \tag{10}$$

In classical approaches, all deterministic parameters are taken into account. Particularly, this means a necessity to consider the nuisance parameters as well since they are considered deterministic. Here, and this motivates the Bayesian approach, it is possible to exclude the nuisance parameters by integration over their pdfs [16]. While analytic computations of integrals may be cumbersome, we exploit properties of the employed Design Of Computer Experiments (DOCE) to implement this.

Although a simplified analytic model is available to describe the relationship of applied force and measured capacitances, the true connection is unknown. From Equation 1 we might already assume a non-linear relationship. To approximate the true deterministic dependence ($g(.)$ in (6)), the so-called forward problem is solved by generating a system model from simulation data. A fast approach [17] is approximating (9) by

$$E\{\theta|y\} = Wy + B \tag{11}$$

to yield the optimal solution, we find

$$W = C_{\theta Y} C_{YY}^{-1} \tag{12}$$

$$B = \bar{\theta} - W\bar{y} \tag{13}$$

where $C_{\theta Y}$ and C_{YY} are covariance matrices of the estimate and the measurement, and of the individual measurements respectively, accounting also for the measurement noise. $\bar{\theta}$ is used to denote the expected value of the parameters to be estimated with respect to their prior distributions. Correspondingly, $\bar{y}$ means the expected value of the measurement.

To find the optimal electrode geometry, we minimize the discrepancy between the estimated and the true force applied to the system. For the target system, three concentric electrode segments with variable inner and/or outer radii, as given in Table 1, are considered. The vector

Table 1. Assignment of electrode parameters and degrees of freedom available to the optimization.

	start radius	end radius
1^{st} electrode	0	r_1
2^{nd} electrode	r_2	r_3
3^{rd} electrode	r_3	r_4

$r_{opt} = [r_{1_{opt}} r_{2_{opt}} r_{3_{opt}} r_{4_{opt}}]^T$ of the optimal combination of radii is then found solving the optimization problem

$$\underset{r_1,r_2,r_3,r_4}{\text{argmin}} \quad Bmse(f, r_{opt}) \tag{14}$$

$$\text{subject to} \quad r_1 < r_2 \tag{15}$$

$$r_2 < r_3 \tag{16}$$

$$r_3 < r_4 \tag{17}$$

$$r_4 < 6\,\text{mm} \tag{18}$$

$$r_1, r_2, r_3, r_4 > 0 \tag{19}$$

4. Design of Computer Experiments

Usually, reliability testing of devices is done after manufacturing of the same and might thus be time-consuming as well as costly [18]. To avoid such an effort in the design of new devices, Finite Element Method (FEM) tools provide a way to analyse and characterize new structures in advance. The employment of FEM analyses, now, comes at the cost of simulation times of several hours up to a few days for large designs. To overcome this drawback, DOCEs are adopted, suitable for the specific aims of the study. Such methodologies enable reduction of the number of necessary computer experiments while providing analytic proofs for the taken samples to be representative for the whole experimental region.

For the analysis of the topology and material variations of the target capacitive sensor, a so-called space-filling or exploratory design [19], i.e. spreading experiments evenly over the range of each particular input, is adapted. In order to design a robust sensor front-end together with the determination of a variation tolerant calibration curve, we aim to provide full coverage of the input-range. Latin Hypercube Designs (LHD) offer favourable properties not only being space filling, but also projective (all significant input factors are sampled equivalently, i.e. there are no clusters) [20]. Defining computer experiments based on an LHD provides advantages over employment of Response Surface Methods (RSM) such as Central Composite Designs (CCDs) or Box-Behnken Designs (BBDs): Beside others (compare [21] and [22]), it allows for sampling from the actual distributions. It aids the Bayesian approach in that we integrate out the influence of the nuisance parameters through the sampling procedure already.

We assume the inputs to be RVs distributed according to a Gaussian distribution, with their mean at the nominal value, and variances given according to manufac-

Table 2. Overview of variable design, nuisance and material parameters and their distribution properties.

Parameter	Symbol	μ	σ	Unit
diaphragm radius	r_{dia}	8	0.2	mm
diaphragm thickness	t_{dia}	0.36	0.02	mm
diaphragm inner radius	r_{in}	6.5	0.2	mm
support thickness	$t_{support}$	0.36	0.02	mm
active diameter	f_{dia}	4	2	mm
active diameter x-offset	f_{xoffs}	0	2	mm
active diameter y-offset	f_{yoffs}	0	2	mm
modulus of elasticity	E_{var}	147	1	GPa
material density	ρ_{var}	7000	300	$\frac{kg}{m^3}$
Poisson ratio	ν_{var}	0.25	0.01	
conductivity	s_{var}	19.68	1	$\frac{MS}{m}$

turer tolerances or geometrical restrictions in case of the variations on boundary conditions respectively. The LHD sample of size N of a random input vector U (as given in [23] and [24]), subject to random deviates $\zeta_{nj}(n = 1,2,...,N; j = 1,2,...,J)$ that are independent and identically distributed uniformly over $[0,1]$, can be found from

$$U_{nj} = F_j^{-1}(\frac{\pi_{nj} - 1 + \zeta_{nj}}{N}) \tag{20}$$

with F_j the marginal distribution of U_j, i.e. component j of vector U, and π_{nj} one element of a NxJ matrix Π which is the column-wise collection of independent random permutations of $\{1,2,...,N\}$. In case of uniformly distributed inputs $u_i \in U$, this procedure is, figuratively spoken, equivalent to splitting the input domain of each u_i into cells where the π_{nj} component determines the cell the input is sampled from and ζ_{nj} specifies its location within the cell (compare also [19]).
In our experiments, we assume a normal distribution of the input variables, i.e. design, nuisance and material parameters as given in Table 2. The uncertainty on geometry variables is taken as specified by the manufacturer [25].

5. Optimization Results

A set of 84 FEM-simulations is generated, each covering a full sample set of the prior distribution of the force. The evolution of the MSE per sample for an optimized array as well as an optimal single electrode structure over increasing considered number of samples is illustrated in Figure 5. The samples are sorted in ascending order according to the magnitude of radial deviation of the applied force from the diaphragm center. Obviously, the MSE for the multi-electrode configuration increases significantly when considering more than 30 samples. Afterwards, the error per sample is rather monotonic, with either sensing structure, for radial deviations up to $\sigma_r \approx 3.4\,\text{mm}$. In the following, again a significant increase until the final $\sigma_r \approx 3.7\,\text{mm}$ can be observed. The arrayed structure exhibits MSE values which are between 37% for small radial deviation to, at least, 95% of those found for a

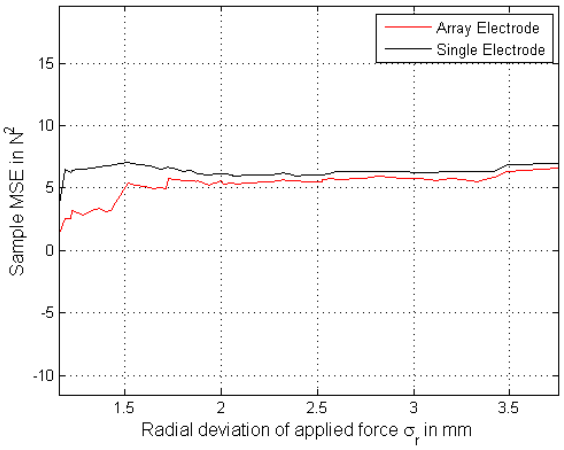

Figure 5. Evolution of the sample-wise MSE over considered samples. The radial deviation from center of the area where force is applied increases with increasing sample number.

single electrode. The lowest errors are attainable at radial deviations below 1.3 mm. We thus restrict the admissible radial variations of force application to $\sigma_r \approx 1.3\,\text{mm}$. For such a configuration, the optimization procedure suggests the optimal electrode structure to be realizable with radii $r_1 = 0.3\,\text{mm}$, $r_2 = 1.1\,\text{mm}$, $r_3 = 1.7\,\text{mm}$ and $r_4 = 2.3\,\text{mm}$, exhibiting a minimal Bayesian mean square error on the force. Specifically, the optimal configuration, as depicted in Figure 6, employs an inner electrode, filling the center, up to a diameter of 0.6 mm, subsequent diameters between 0.6 mm and 2.2 mm are uncovered, then the second electrode follows, covering diameters between 2.2 mm and 3.4 mm, the third electrode is arranged at diameters from 3.4 mm to 4.6 mm. For this configuration the error $MSE_{opt} = 1.3\,\text{N}^2$ can be found, which is, at this point, 37% of the MSE with measurement of only one electrode. In Figure 7 the estimated force is plotted against the true applied force for all considered samples. While a linear relation is expected, we find a remaining non-linear discrepancy for which the estimator does not completely compensate. To reason this, we further examine the basis sample set: although the considered set is reduced to samples at feasible radii, the variations in diameter of the applied force are not restricted and are supposed to exert this strong influence causing the non-linearity.
The diaphragm design exhibits the highest sensitivity for force applied directly at its center. Thus, it seems intuitively logical that discretization of this region of highest sensitivity together with disregarding influences outside the permissible radius, is favourable to simpler configurations. Employing multiple variable concentric electrodes enables adaptation to various demands with respect to considered diameter as well as radial variations.

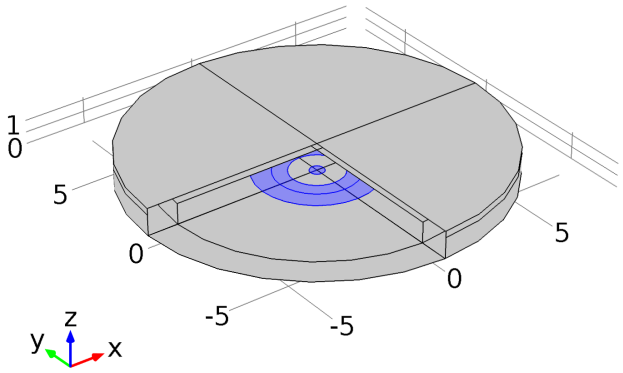

Figure 6. Full system geometry where a quarter of the diaphragm is hidden to reveal the optimal electrode configuration (blue-coloured surfaces).

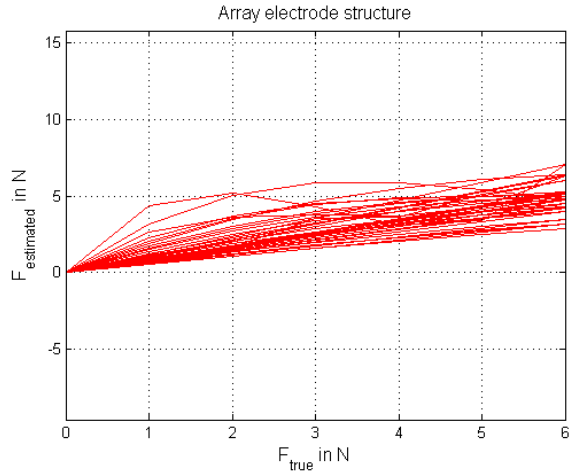

Figure 7. Estimated force is plotted versus true force for all considered samples, for certain samples a remaining non-linearity can be observed.

6. Conclusion

We presented the application of an LHD, closely linked to the subsequent Bayesian approach for a robust 3D- and inkjet printed pressure sensor. The degrees of freedom for the considered system were explained and the way they were taken into account was outlined for the design of experiments as well as for the Bayesian approach to optimal system calibration.

Two different capacitive sensing concentric electrode structures were studied and optimized based on a set of LHD samples, and their performance was evaluated based on the BMSE as performance metric. The superiority of the multi-electrode structure was shown over the complete sample set. Additionally, the optimal electrode configuration was illustrated for a reduced set, restricted to feasible radial deviations in the area of applied force. When highly non-centric force application is to be expected, the introduction of additional degrees of freedom with respect to electrode shape is suggested to be considered for improved performance. A future aim lies in the study of such other geometrical configurations.

While measurements have already been done validating the simulation results for a single electrode sensor structure, validation and evaluation of the optimal configuration may substantiate the results presented here in further work.

Acknowledgment

This project has been supported by the COMET K1 ASSIC Austrian Smart Systems Integration Research Center. The COMET-Competence Centers for Excellent Technologies-Programme is supported by BMVIT, BMWFW and the federal provinces of Carinthia and Styria.

References

[1] J. Lee, H. Kwon, J. Seo, S. Shin, J. H. Koo, C. Pang, S. Son, J. H. Kim, Y. H. Jang, D. E. Kim *et al.*, "Conductive fiber-based ultrasensitive textile pressure sensor for wearable electronics," *Advanced Materials*, vol. 27, no. 15, pp. 2433–2439, 2015.

[2] A. M. Almassri, W. Wan Hasan, S. Ahmad, A. Ishak, A. Ghazali, D. Talib, and C. Wada, "Pressure sensor: state of the art, design, and application for robotic hand," *Journal of Sensors*, vol. 2015, 2015.

[3] A. Aldaoud, C. Laurenson, F. Rivet, M. R. Yuce, and J.-M. Redouté, "Design of a miniaturized wireless blood pressure sensing interface using capacitive coupling," *Mechatronics, IEEE/ASME Transactions on*, vol. 20, no. 1, pp. 487–491, 2015.

[4] S. Lee, A. Reuveny, J. Reeder, S. Lee, H. Jin, Q. Liu, T. Yokota, T. Sekitani, T. Isoyama, Y. Abe *et al.*, "A transparent bending-insensitive pressure sensor," *Nature nanotechnology*, 2016.

[5] A. J. Fleming, "A review of nanometer resolution posiition sensors: Operation and performance," *Sensors and Actuators, A: Physical*, 2013.

[6] L. Baxter, *Capacitive Sensors, Design and Applications*. IEEE Press, 1997.

[7] A. Panesar, D. Brackett, I. Ashcroft, R. Wildman, and R. Hague, "Design optimization strategy for multifunctional 3d printing," in *25th Interational Solid Freeform Fabrication Symposium*, 2014.

[8] B. Ando and S. Baglio, "Inkjet-printed sensors: a useful approach for low cost, rapid prototyping [instrumentation notes]," *Instrumentation & Measurement Magazine, IEEE*, vol. 14, no. 5, pp. 36–40, 2011.

[9] R. Popovic and J. Flanagan, "Sensor microsystems," *Microelectronics Reliability*, vol. 37, 1997.

[10] W. C. Dunn, *Introduction to Instrumentation, Sensors, and Process Control*. Artech House, Boston, 2005.

[11] G. Brasseur, "Design rules for robust capacitive sensors," *IEEE Transactions on Instrumentation and Measurement*, 2003.

[12] V. Kaajakari, *Practical MEMS*. Small Gear Publishing, 2009.

[13] L. L. Faulkner, Ed., *Microengineering, MEMS, and Interfacing*. Taylor and Francis Group, LLC., 2006.

[14] S. Beeby, G. Ensell, M. Kraft, and N. White, *MEMS Mechanical Sensors*. Artech House, Boston, 2004.

[15] (2016, Feb.) Comsol multiphysics documentation, version 5.2.

[16] S. M. Kay, *Fundamentals of Statistical Signal Processng, Estimation Theory*. Prentice-Hall, Inc., 1993.

[17] J. Bardsley, "Mcmc-based image reconstruction with uncertainty quantification," *SIAM Journal on Scientific Computing*, vol. 34, no. 3, pp. A1316–A1332, 2012.

[18] B. Bergman, de MarÃ© J., S. LorÃ©n, and T. Svensson, Eds., *Robust Design Methodology for Reliability*. John Wiley & Sons, Ltd., 2009.

[19] T. J. Santner, B. J. Williams, and W. I. Notz, *The Design and Analysis of Computer Experiments*. Springer Verlag New York, 2003.

[20] N. Vollert, J. Schicker, C. Hirschl, M. Kraft, and J. Pilz, "Designing efficient computer experiments - the step beyond finite element modelling," in *Thermal, Mechanical and Multi-Physics Simulation and Experiments in Microelectronics and Microsystems (EuroSimE), 2015 16th International Conference on*, 2015.

[21] G. Pan, P. Ye, P. Wand, and Z. Yang, "A sequential optimization sampling method for metamodels with radial basis functions," *Scientific World Journal*, 2014.

[22] J. Sacks, W. J. Welch, T. Mitchell, and H. P. Wynn, "Design and analysis of computer experiments," *Statistical Science*, vol. 4, no. 4, pp. 409–435, 1989.

[23] M. D. McKay, W. J. Conover, and R. J. Beckman, "A comparison of three methods for selecting values of input variables in the analysis of output from a computer code," *Technometrics*, 1979.

[24] M. Stein, "Large sample properties of simulations using latin hypercube sampling," *Technometrics*, 1987.

[25] (2016, Feb,). [Online]. Available: https://i.materialise.com/materials/high-detailed-stainless-steel/design-guide